Liquid-Ordered Phase Formation in Cholesterol/Sphingomyelin Bilayers: All-Atom Molecular Dynamics Simulations

ARTICLE *in* THE JOURNAL OF PHYSICAL CHEMISTRY B · DECEMBER 2009

Impact Factor: 3.3 · DOI: 10.1021/jp907138h · Source: PubMed

7 AUTHORS, INCLUDING:

Franci Merzel
National Institute of Chemistry
42 PUBLICATIONS **666** CITATIONS
SEE PROFILE

Katja Rebolj
National Institute of Chemistry
14 PUBLICATIONS **203** CITATIONS
SEE PROFILE

Kristina Sepcic
University of Ljubljana
125 PUBLICATIONS **2,081** CITATIONS
SEE PROFILE

Peter Maček
University of Ljubljana
124 PUBLICATIONS **4,069** CITATIONS
SEE PROFILE

Liquid-Ordered Phase Formation in Cholesterol/Sphingomyelin Bilayers: All-Atom Molecular Dynamics Simulations

Jernej Zidar,[†] Franci Merzel,[†] Milan Hodošček,[†] Katja Rebolj,[‡] Kristina Sepčić,[‡] Peter Maček,[‡] and Dušanka Janežič*,[†]

National Institute of Chemistry, Hajdrihova 19, SI-1000 Ljubljana, Slovenia, and Department of Biology, Biotechnical Faculty, University of Ljubljana, Večna pot 111, SI-1000 Ljubljana, Slovenia

Received: July 27, 2009; Revised Manuscript Received: October 16, 2009

This paper reports an all-atom molecular dynamics simulation of lipid bilayers with different cholesterol/sphingomyelin molar ratios. Our results reveal structural and dynamic changes suggesting the random distribution of lipids along the bilayer planes is supplanted at cholesterol concentrations above 30 mol % by the formation of a liquid-ordered phase, which is thought to be the precursor to lipid raft formation. The packing of molecules in the bilayer is shown to be associated with the hydrogen bonding between cholesterol and sphingomyelin. The molecules tend to migrate toward distributions in which the sphingomyelin molecule forms on average one hydrogen bond with a cholesterol molecule. The threshold for activation of this packing trend coincides with the experimentally determined threshold membrane activity of a cytolytic protein ostreolysin, which binds to and permeabilizes cholesterol−sphingomyelin bilayers containing more than 30 mol % cholesterol.

Introduction

The plasma membrane is a lipid bilayer composed of many membrane domains, whose existence depends on the lipid composition. In this model, certain membrane lipids, in particular sterols, are responsible for the separation of membrane lipid domains into coexisting liquid-disordered (l_d) and liquid-ordered (l_o) phases.[1] Lipids in the l_o domains are tightly packed, but capable of rapid lateral diffusion, and are usually more resistant to solubilization by detergents than lipids in the l_d domains.[2] The l_o domains are thicker than those elsewhere in the membrane[3] and are the basis of lipid rafts, which are membrane microdomains enriched in sphingolipids, cholesterol, and specific proteins.[4] Lipid rafts are believed to be transient, dynamic, and unstable nanoscale clusters[5,6] of different sizes[7] but can be stabilized by binding ligand molecules.[5,8,9] They are known to be involved in several important biological functions, such as membrane trafficking, signal transduction, pathogen entry, and attachment of various ligands.[10−12]

A plethora of cytolytic proteins have been shown to interact with raft-like domains.[13,14] Recently, a cytolytic protein, ostreolysin, was found specifically to sense the heterogenic distribution of cholesterol in biological membranes. This 15 kDa acidic protein, found in large amounts in young fruiting bodies of the edible oyster mushroom (*Pleurotus ostreatus*),[16,17] is functionally classified as a new member of the cholesterol-dependent cytolysin family.[18] In contrast to many other members of this group, it cannot bind pure cholesterol or any other molecule abundant in lipid rafts, but it interacts exclusively with lipid membranes in which cholesterol is combined with sphingomyelin or with fully saturated glycerophospholipids.[19] Several lines of evidence support the specific interaction of ostreolysin with raft-like domains. In particular, ostreolysin binds to, and permeabilizes membranes composed of sphingomyelin and cholesterol only when the cholesterol level is above 30 mol %,[19] i.e., at concentrations at which the formation of a l_o phase[20] is induced. At cholesterol levels of up to 60 mol %, the membrane activity of ostreolysin is enhanced in a highly cooperative manner as shown in Figure 1, which resumes the experimental results of the previous work by Rebolj et al.[18] and Sepčić et al.[19] It is hypothesized that the critical condition for ostreolysin binding to biological membranes and lipid bilayers is the prior existence of raft-like domains in the lipid bilayer.

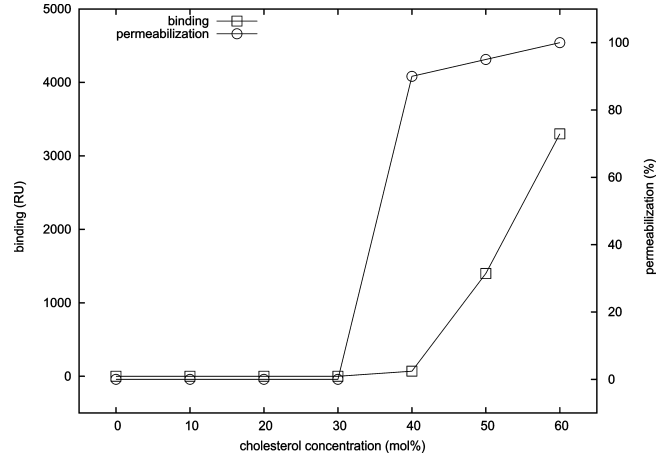

Figure 1. Effect of cholesterol/sphingomyelin ratio on ostreolysin membrane activity. Binding (squares) of 55 μM ostreolysin was assessed on cholesterol/sphingomyelin monolayers coupled to a Sensor Chip HPA using the surface plasmon resonance technique. The binding signal is expressed in resonance units (RU), corresponding to the response of bound ostreolysin after subtracting the fitted bulk component. Permeabilization (circles) was studied spectrofluorimetrically by applying ostreolysin (3.96 μM) to calcein-loaded cholesterol/sphingomyelin sonicated unilamellar vesicles, and the percentage of release of the fluorescent dye was calculated. Both experiments (binding and permeabilization) were performed at 25 °C using the same lipid/protein molar ratio of 9.09. Adapted from Rebolj et al.[18,19]

* Corresponding author. Tel.: +(386)1-476-0321. Fax: +(386)1-476-300. E-mail: dusa@cmm.ki.si.
[†] National Institute of Chemistry.
[‡] University of Ljubljana.

10.1021/jp907138h CCC: $40.75
Published on Web 11/06/2009

To detect structural modifications in the cholesterol-containing sphingomyelin bilayers resulting from increases in the proportion of cholesterol and possibly related to the early steps of lipid raft formation, we have performed molecular dynamics simulations of different bilayers composed of cholesterol and sphingomyelin molecules in 20/80, 30/70, 35/65, and 40/60 molar ratios. For comparison, we simulated also a pure sphingomyelin(18:0) bilayer. Of particular interest are any differences that would appear in bilayers containing approximately 30 mol % cholesterol, the concentration found to be the threshold for the membrane activity of ostreolysin.[18,19]

Some of the effects of cholesterol on bilayer dynamics occur on time and space scales not easily within reach of current molecular dynamics simulations at the atomic level, but several groups have used atomic and mesoscopic simulations to investigate the structural and dynamic characteristics of phospholipid/cholesterol systems.[22−26] In model systems composed of cholesterol and sphingomyelin, molecular dynamics[27] simulations have been shown to be an invaluable tool for the study of lipid bilayer organization,[28−32] and in many cases the simulations confirmed experimental results. Raft-like domains composed of sphingomyelin and cholesterol in a 2/1 molar ratio were found to enhance the ordering of the surrounding dioleoylphosphatidylcholine matrix, which becomes 4.5 Å thicker than the remainder of the bilayer,[33] and to have similar thickness, structure, and ordering characteristics at both 20 and 50 °C.[34] In sphingomyelin/cholesterol/dioleoylphosphatidylcholine mixtures, cholesterol was shown to accelerate the process of domain formation.[35] Recent molecular dynamics simulations of cholesterol/sphingomyelin lipid bilayers revealed that even a single cholesterol molecule could cause local bilayer ordering and condensation.[36] Such simulations of raft-containing palmitoyloleyl-phosphatidylcholine/cholesterol/sphingomyelin bilayers also revealed considerable heterogeneity on the 10−100 ns scale within the raft domains and the ability of cholesterol to alter the lateral pressure in lipid bilayers.[37]

The aim of this work was to provide insight into the structural organization and redistribution of ostreolysin-susceptible cholesterol−sphingomyelin(18:0) bilayers, such redistribution being crucial in the formation of the liquid-ordered phase. For our simulation studies, the two lipid layers were randomly populated with either sphingomyelin or cholesterol molecules in the chosen molar ratio. Simulation times of several tens of nanoseconds of all-atom molecular dynamics were expected to provide satisfactory relaxation of the system and to reveal the tendencies for mixing and packing of lipids in response to the increased concentration of cholesterol.

Methods

Five hydrated all-atom lipid bilayers were built with molar cholesterol/sphingomyelin(18:0) ratios of 0/100 (pure sphingomyelin), 20/80, 30/70, 35/65, and 40/60, through a multistep process as follows.

a. Construction of Cholesterol and Sphingomyelin Molecules. The cholesterol molecule was built with available CHARMM topology and parameter data.[45−47] In our study, we have selected sphingomyelin(18:0) (Figure 2), which is known to be most frequently found in nature. The sphingomyelin(18:0) molecules were built from a related molecule, 1,2-dimyristoyl-*sn*-glycero-3-phosphocholine, by an analogy approach.[45−47] The sphingomyelin molecules constructed in this way and the cholesterol model are displayed in Figure 2.

b. Construction of Lipid Bilayers. Five lipid bilayer models were constructed with the sphingomyelin(18:0) and cholesterol

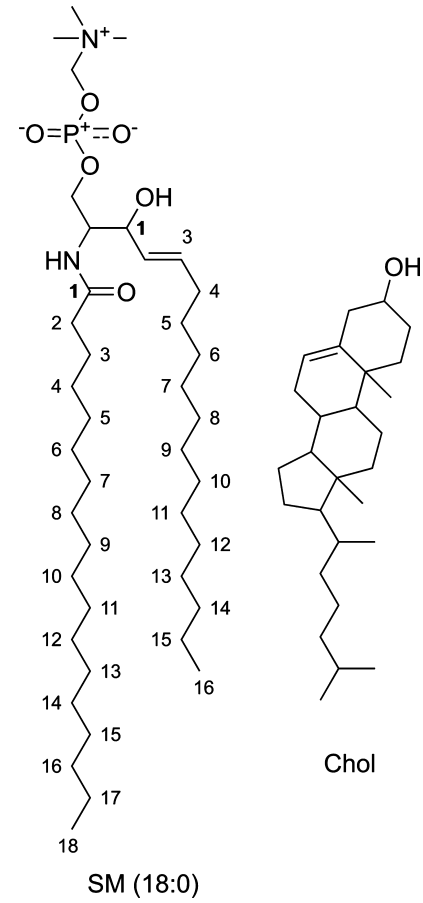

Figure 2. Structure of sphingomyelin(18:0) and cholesterol molecule used in the simulations. The exact orientation around the chiral atoms is omitted for clarity, and the superscripts (+ or −, respectively) near some atoms denote the atomic charge of those atoms.

structures. Two parallel layers were first populated with 400 (i.e., 200 beads per layer) spherical beads, whose size approximates the size of the lipid molecule polar head. These two layers were then shrunk to 95 × 95 Å using the Steepest Descent (SD) minimization algorithm[38] followed by 100 ps of Langevin dynamics at 300 K.

In the next step, each spherical bead was randomly replaced using the methodology from refs 28, 38, 39, and 43 with either a sphingomyelin(18:0) or a cholesterol molecule to conform to the desired cholesterol/sphingomyelin molar ratio. The hydrophobic parts of sphingomyelin and cholesterol molecules were oriented toward the inside of the bilayer. These models were then gradually minimized using the SD algorithm by slowly increasing the van der Waals radii of the atoms.

The top and bottom parts of the lipid bilayer models were covered with TIP3P[40] water molecules, previously minimized using the SD algorithm and adopted-base Newton−Raphson algorithm (ABNR),[38] to give an approximate ratio of 25 water molecules per lipid molecule. The exact numbers of cholesterol, sphingomyelin, and water molecules in each unit cell are given in Table 1. The overall unit cell size was initially set to 95 × 95 × ∼72 Å containing approximately 70 000 atoms, 24 900 of which were water atoms.

c. Equilibration and Production Run. These system were further subjected to ABNR minimization and extensive equilibration with 30 ns molecular dynamics runs at constant temperature (300 K) and pressure (1 atm) using the Hoover method.[41] The unit cell size was allowed to change only along the *z*-axis for the first 5 ns; this constraint was removed in the

TABLE 1: Summary of Model Bilayer Data

cholesterol/sphingomyelin molar ratio	number of molecules in unit cell		
	cholesterol	sphingomyelin	water
0/100	0	400	12628
20/80	80	320	8907
30/70	120	280	9537
35/65	140	260	9863
40/60	160	240	9422

remaining simulation. Electrostatics were treated by the Particle Mesh Ewald algorithm.[42] The distance cutoff was set to 14.0 Å. The distance at which the switching function eliminates all contributions from a pair in calculating energies was set to 10.0 Å, and the distance at which the smoothing function begins to reduce a pair's contribution was set to 7.0 Å. The molecular dynamics production runs were 30 ns long. Simulation of pure sphingomyelin(18:0), which was used for comparison, was 10 ns long.

Trajectories generated for each lipid bilayer system with the time step of 1 fs were used for analysis of the following properties of lipid bilayers: electron density profiles, mean square displacements, chain order parameter for acyl and sphingosine chains of sphingomyelin(18:0), radial distribution functions, and nearest neighbor analysis between cholesterol and sphingomyelin molecules.

Molecular dynamics simulations[43,44] were performed with the CHARMM[38,43] biomolecular simulation program, version c33a1, using the CHARMM27 all-atom parameter set.[45−47] All simulations were run on the CROW[48] computer cluster at the National Institute of Chemistry, Ljubljana, Slovenia. The various lipid bilayer systems were visualized using VMD.[49]

Results and Discussion

The aim of this work was a study of lipid bilayers with different cholesterol/sphingomyelin molar ratios using molecular dynamics simulations. Five different fully hydrated ensembles, corresponding to cholesterol/sphingomyelin(18:0) molar ratios of 0/100, 20/80, 30/70, 35/65, and 40/60 were constructed. Simulations were run to find changes in the structural organization of cholesterol/sphingomyelin(18:0) model bilayers as the cholesterol concentration varied. Figure 3 shows the top views of different systems (Figure 3a−c) and the side view of the bilayer unit with cholesterol/sphingomyelin(18:0) in a 35/65 ratio (Figure 3d).

In a number of recently published simulation and experimental studies on cholesterol/sphingomyelin mixtures, it has been shown that increasing concentrations of cholesterol promote the ordering of the acyl chains of sphingomyelin and subsequently lead to different packing of sphingomyelin. These results suggest that simulations can contribute to the understanding of how the addition of cholesterol affects the phospholipid properties in the plasma membrane.

To validate our simulation protocol we first check the structural and dynamical properties of the lipid bilayers by computing their electron density profiles and diffusion constants. To determine the width of the bilayer the total electron density profiles were calculated by counting the partial charges of the bilayer atoms in different lateral slices divided by the volume of the slice and averaged across the entire 30 ns production runs. Total electron density profiles for each composition ratio are shown in Figure 4a as a function along the z axis of the bilayer, where $z = 0$ corresponds to the "mirror" plane. All curves in Figure 4a have the following features in common: an external plateau when z is approximately ±30 Å, a peak centered around ±23 Å, a shoulder for $z \pm 10$ Å, and a minimum at the center ($z = 0$). The intensity of the peaks at z of approximately ±23 Å increases with decreasing amounts of cholesterol. The distance between these peaks is approximately 46 Å which is in agreement with previous simulation[25] and experimental[50] data for the bilayer width. These two symmetric peaks are due to the polar groups of sphingomyelin molecules in both lipid layers. This can be confirmed by partial electron density profiles for each component of the lipid bilayer, plotted in Figure 4b for the lipid bilayer containing 35 mol % of cholesterol. The level of equilibration was assessed by calculating the partial electron density profiles for the first 5 ns and the last 5 ns of the 30 ns production run (in Figure 4b). Each lipid bilayer system has three components: cholesterol, sphingomyelin, and water. The electron density of cholesterol is found to be confined to the values where z is ±20 Å which is assumed to be the consequence of a strong interaction between the sphingomyelin polar head groups and cholesterol. The comparison of the curves in Figure 4b shows that the differences in electron density distributions are minor suggesting our production run covers a well-equilibrated part of the simulation.

The dynamical properties of the lipid bilayers were checked by measuring the mean square displacements (MSD), $<r^2(t)>$ (t is the production simulation time), of sphingomyelin molecule centers of mass shown in Figure 5. Diffusion constants were calculated using the Einstein relation

$$D(t) = \lim_{t\to\infty} \frac{<r^2(t)>}{4t} \quad (1)$$

The calculated short-time (5 ns) diffusion constants from 30 ns of the production run are in the range $D = 0.25-0.5$ Å^2/ns corresponding to 20−40 mol % of cholesterol, which is in good agreement with the experimentally measured diffusion constants for sphingomyelin.[24]

The electron density profiles and diffusion constants obtained from our simulation data indicate the CHARMM force field and our simulation protocol adequately account for the structural and dynamic features of the cholesterol/sphingomyelin bilayers.

To quantify the level of ordering for compositions corresponding to different concentrations of cholesterol, we calculated the C−H chain order parameter (S_{CH}), which measures the mobility of the C−H bond and is defined in eq 2

$$S_{CH} = \frac{1}{2}(3 < \cos^2 \theta_{CH} > -1) \quad (2)$$

where θ_{CH} is the angle between a C−H bond and the normal to the bilayer.[51] The lower the value of S_{CH}, the greater is the rotation of the C−H bond around the bilayer normal. The maximal S_{CH} value of zero indicates an unordered system, where the directions of the C−H bonds are isotropic, while the minimal S_{CH} value of −0.5 indicates a perfectly ordered system (completely aligned C−H bonds). Going from the bilayer interface to the bilayer center, the chain order parameter decreases. Calculated S_{CH} parameters for different C-atoms along the sphingosine and acyl chains in the sphingomyelin are shown in Figure 6a and Figure 6b, respectively. The lipid tails of sphingomyelin belonging to the ensembles in which the cholesterol concentration is greater or equal to 30 mol % (blue, violet, and cyan curves in Figure 6) are more ordered than those with 0 and 20 mol % cholesterol (red and green curves), which

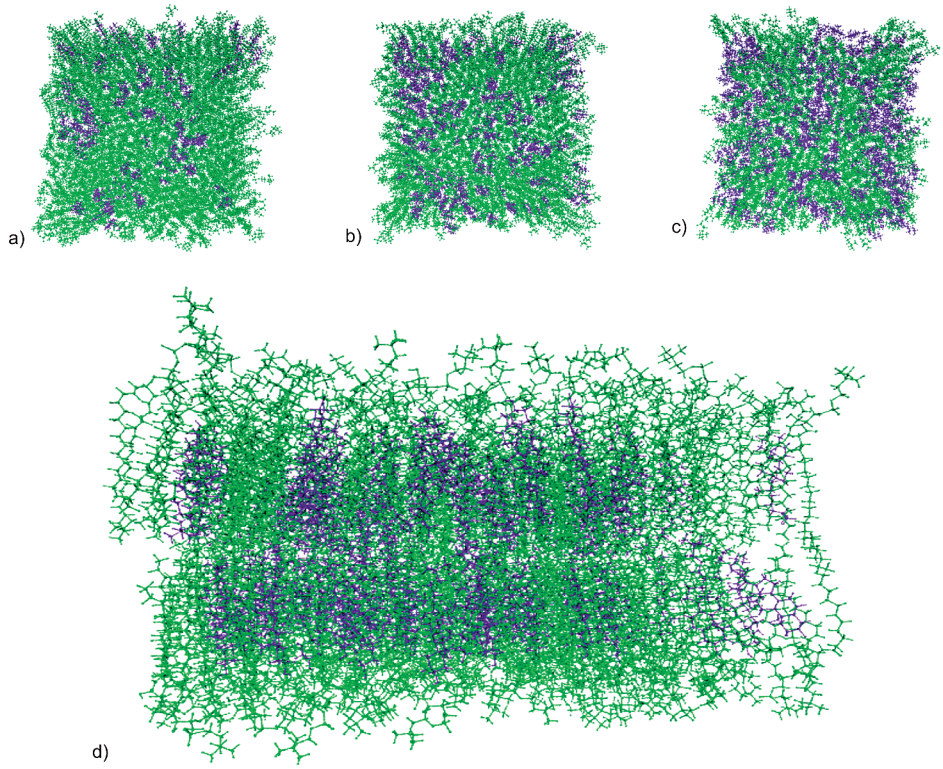

Figure 3. Top view of bilayers with the following cholesterol (violet)/sphingomyelin(18:0) (green) molar ratios: (a) 20/80, (b) 35/65, and (c) 40/60. (d) Side view of the model system with cholesterol/sphingomyelin(18:0) ratio of 35/65. Water molecules are omitted for clarity reasons.

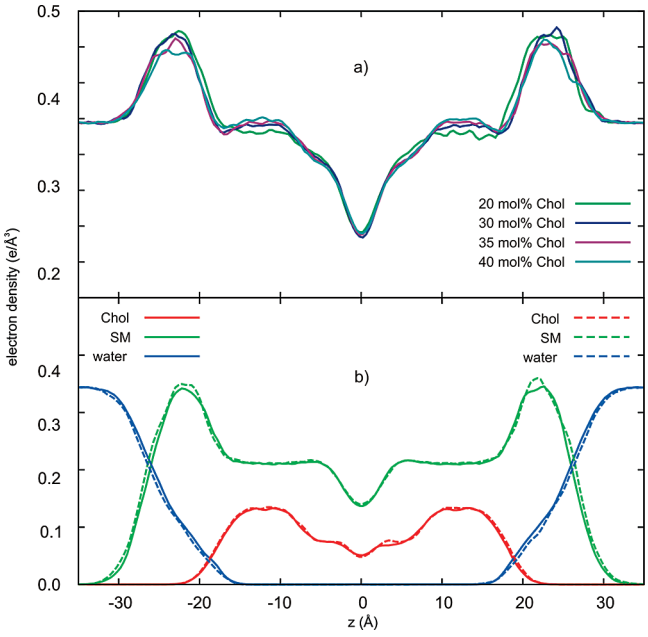

Figure 4. (a) Total electron density profiles in lipid bilayers with different cholesterol/sphingomyelin(18:0) molar ratios. Key: green, 20 mol % cholesterol; blue, 30 mol % cholesterol; violet, 35 mol % cholesterol; cyan, 40 mol % cholesterol. (b) Electron density profiles for the components of lipid bilayer with 35 mol % cholesterol. Solid lines correspond to the first 5 ns and dashed lines to the last 5 ns of the 30 ns production run, and z is the distance to the center of the membrane. Key: red, cholesterol; blue, water; green, sphingomyelin.

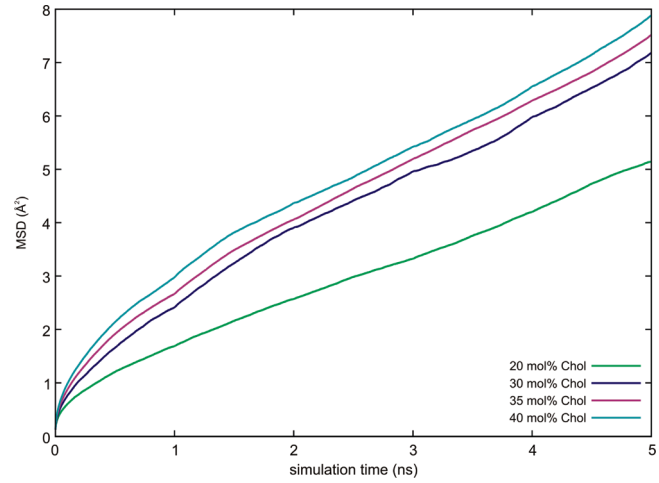

Figure 5. Mean square displacements (MSD) in Å^2 for the sphingomyelin(18:0) molecule. Key: green, 20 mol % cholesterol; blue, 30 mol % cholesterol; violet, 35 mol % cholesterol; cyan, 40 mol % cholesterol.

is confirmed by the curves being located in two distinct groups: one below 30 mol % of cholesterol and another above 30 mol % of cholesterol. This suggests the possibility of two different regimes of ordering: one at cholesterol concentrations below 30 mol % with the characteristics of the so-called l_d phase and the other at or above 30 mol % cholesterol corresponding to the l_o phase, which is assumed to be a precursor of the raft-like domain. An indication for existence of two phases in the cholesterol−sphingomyelin bilayer as a result of the variation of cholesterol concentration is thus reproduced.

Rearrangements associated with phase transitions inside the bilayer can also be detected by calculating radial distribution functions (RDF). In Figure 7, the RDF functions for the mass centers of the sphingomyelin polar heads are shown, displaying the arrangement of sphingomyelin molecules in the bilayer. For each cholesterol concentration, a pronounced first coordination shell is centered at distances of approximately 7−8 Å, where we also observe a good signal-to-noise ratio. As the concentration of cholesterol increases from 20 to 30 mol %, the position of the peak changes, but increasing the concentration above 30

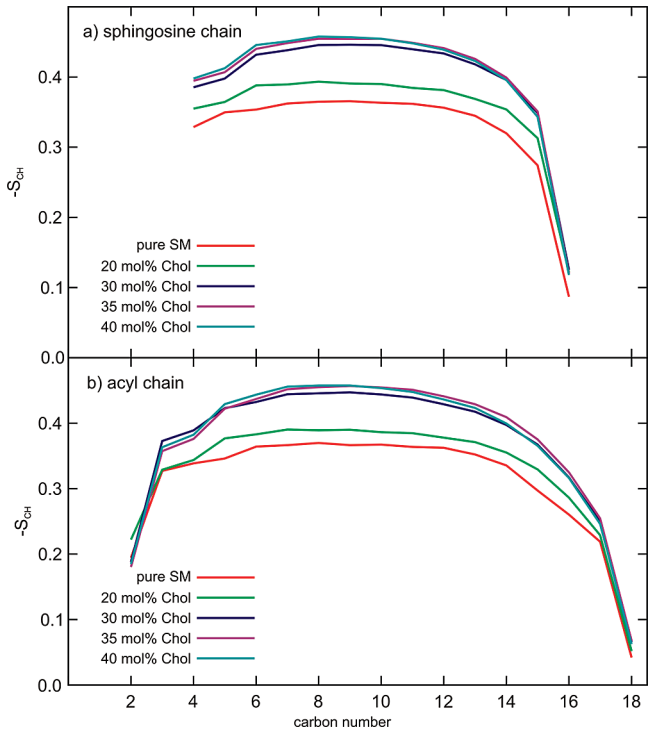

Figure 6. Chain order parameter (S_{CH}) results for sphingomyelin(18:0): (a) for the sphingosine chain and (b) for the acyl chain of sphingomyelin(18:0). Key: red, pure sphingomyelin; green, 20 mol % cholesterol; blue, 30 mol % cholesterol; violet, 35 mol % cholesterol; cyan, 40 mol % cholesterol.

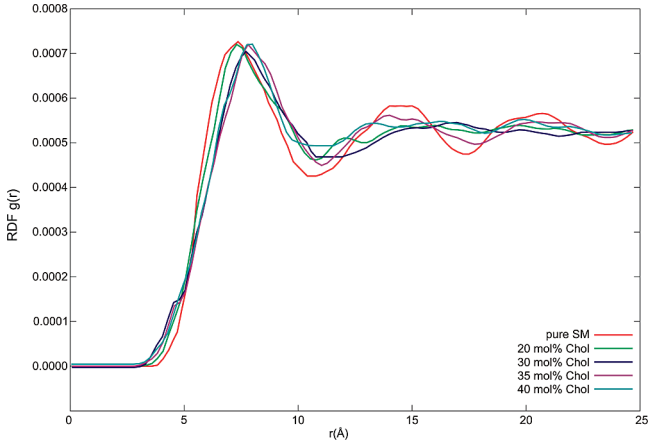

Figure 7. Radial distribution functions (RDF) for the mass centers of sphingomyelin(18:0) polar heads. Key: red, pure sphingomyelin; green, 20 mol % cholesterol; blue, 30 mol % cholesterol; violet, 35 mol % cholesterol; cyan, 40 mol % cholesterol.

mol % induces no further change. Thus the structural feature that is established at 30 mol % is conserved at higher cholesterol concentrations. The shift of the first RDF peak by approximately 1 Å toward larger values of the RDF for cholesterol concentrations above 30 mol % indicates a type of packing different from that seen at concentrations below 30 mol %.

The ability of cholesterol to form hydrogen bonds with sphingomyelin is a driving force in liquid-ordered phase formation in cholesterol/sphingomyelin bilayers, and hydrogen bonding involving the cholesterol hydroxyl group is thought to play an important role in stabilizing the position of the cholesterol along the nonpolar tails of sphingomyelin (Figure 8). The hydroxyl group of cholesterol can act as both a hydrogen bond donor and a hydrogen bond acceptor with respect to the

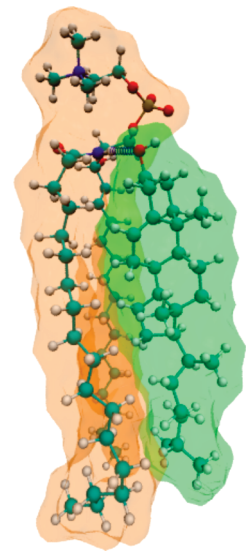

Figure 8. Sphingomyelin(18:0) (orange) molecule interacting with cholesterol (green) molecule.

TABLE 2: Average Number of Hydrogen Bonds between Sphingomyelin(18:0) and Cholesterol Per Cholesterol Molecule for Different Cholesterol/Sphingomyelin Ratios Calculated According to the Distance Criteria

cholesterol/sphingomyelin molar ratio	hydrogen bonds per cholesterol
20/80	0.49 ± 0.03
30/70	0.51 ± 0.02
35/65	0.46 ± 0.02
40/60	0.39 ± 0.02

carbonyl oxygen atom, the hydroxyl group, the four oxygen atoms of the phosphate, any of which can be involved in hydrogen bonding, or the amide groups of sphingomyelin molecules. The average number of hydrogen bonds per cholesterol as a function of cholesterol concentration is shown in Table 2. This shows that the average number of hydrogen bonds per cholesterol is maximized at 30 mol % cholesterol, implying that optimal hydrogen-bonding packing is seen at this concentration. Increasing the cholesterol concentration above 30 mol % vitiates hydrogen bonding because as a result of steric crowding between cholesterol molecules competing for hydrogen bonding to sphingomyelin the number of cholesterol molecules around sphingomyelin becomes too high to satisfy the conditions for hydrogen bond formation. At cholesterol concentrations below 30 mol %, the number of available cholesterol molecules is too small to provide optimum hydrogen bonding. Further assessment of hydrogen bonding was made by checking the number of hydrogen bonds between the donor cholesterol hydroxyl group and acceptor sphingomyelin groups, i.e., the oxygen atoms in the phosphate group (O11, O12, O13, O14), the nitrogen (N21) and oxygen atom (O22) in the amide group, and the oxygen atom (OX) in the hydroxyl group. Table 3 gives the contributions of each donor−acceptor pair to the average number of hydrogen bonds between cholesterol and sphingomyelin molecules. The main contributions to the average number of hydrogen bonds are from the bonds formed between the cholesterol hydroxyl oxygen and the carbonyl oxygen of the amide group or from the hydroxyl oxygen group of the sphingomyelin molecule. This finding is in agreement with the hydrogen bonding scheme presented in Figure 8.

Locally, each sphingomyelin molecule enjoys surroundings which are dictated by the number of cholesterol molecules in

TABLE 3: Number of Hydrogen Bonds between the Cholesterol Donor Atom (Label O3) and Sphingomyelin(18:0) Acceptor Atoms (Labels O11, O12, O13, O14, O22, OX) in the 30 ns Production Runs Averaged over the Number of Cholesterol Molecules in Each Lipid Bilayer

Chol−SM	20 mol % Chol	30 mol % Chol	35 mol % Chol	40 mol % Chol
O3−N21	0.035	0.021	0.026	0.016
O3−O11	0.004	0.009	0.002	0.003
O3−O12	0.002	0.000	0.004	0.003
O3−O13	0.087	0.053	0.060	0.064
O3−O14	0.082	0.091	0.077	0.081
O3−O22	0.157	0.184	0.171	0.153
O3−OX	0.151	0.164	0.118	0.065
average number of hydrogen bonds	0.500	0.522	0.458	0.385

the first coordination shell as shown in Figure 9. The local environment of individual molecules varies with the cholesterol concentration, and analysis of the distribution of cholesterol molecules in the first coordination shell around the sphingomyelin molecules can provide some insight into local packing. Distributions of the average numbers of cholesterol molecules within a radius of 7 Å around sphingomyelin are shown in Figure 10a. Here the distance between sphingomyelin and cholesterol is defined as the separation of the sphingomyelin polar head center of mass from the hydroxyl oxygen of cholesterol. This plot shows qualitative difference for distributions below and above 30 mol % cholesterol. On average, at cholesterol concentrations above 30 mol %, each individual sphingomyelin molecule is most likely to be surrounded by one cholesterol molecule, but at concentrations below 30 mol % it is likely to have only other sphingomyelin molecules as neighbors.

The interaction energy of an individual sphingomyelin molecule with cholesterol is expected to depend on the average number of cholesterol molecules in its immediate vicinity. Decomposition of the interaction energy into electrostatic and Lennard-Jones contributions is the subject of further studies. For a given bilayer composition, differences in interaction energies in various environments should give rise to enthalpic driving forces for molecular redistribution.

To assess the relative values of the interaction energies, we calculated the average interaction energy per sphingomyelin molecule with its surroundings as a function of the number of cholesterol neighbors in the first coordination shell at different molar concentrations of cholesterol. Results are shown in Figure 10b. The average interaction energy curves at cholesterol concentrations above 30 mol % are all "V"-shaped with a minimum at one cholesterol neighbor on average in the first coordination shell, while the average interaction energies for 20 mol % cholesterol turn out to be roughly independent of the number of cholesterol neighbors. The minimum at one cholesterol neighbor means that the interaction of sphingomyelin molecules with their surroundings is strongest when they are on average surrounded by one cholesterol molecule. Thus, the interaction energy of a sphingomyelin molecule with its local environment becomes less favorable when the average number of cholesterol molecules is greater or less than one, which is consistent with the hydrogen bonding data presented in Table 2. The resulting potential difference would then direct an individual sphingomyelin molecule toward the environment containing an optimal number of cholesterol molecules. Also, the average interaction energies for 20 mol % cholesterol shown in Figure 10b are weaker then the average interaction energies in bilayer models with cholesterol concentration above 30 mol %.

Short-range interactions such as hydrogen bonds appear to be critical for liquid-ordered phase formation in cholesterol/sphingomyelin bilayers. The dependency of sphingomyelin interaction energies on the number of cholesterol neighbors is similar for all systems belonging to the liquid-ordered phase examined in our study and is independent of the overall bulk concentration of cholesterol. Thus the driving force for lipid packing in the bilayers is determined by the immediate environment of the sphingomyelin molecules, i.e., on short-range interactions.

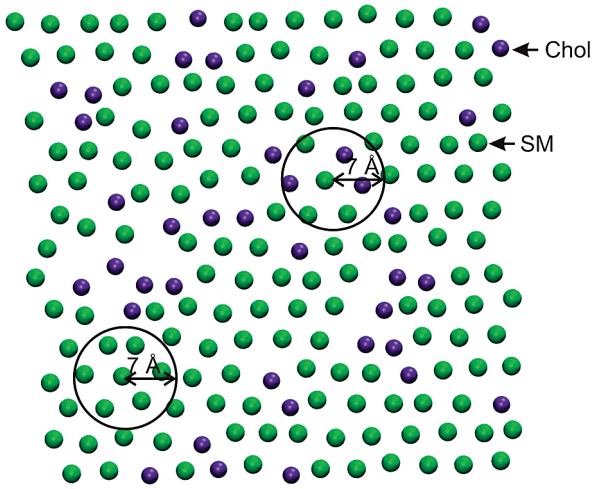

Figure 9. Schematic representation of the way the number of nearest cholesterol (violet) neighbors of sphingomyelin(18:0) (green) molecules was determined.

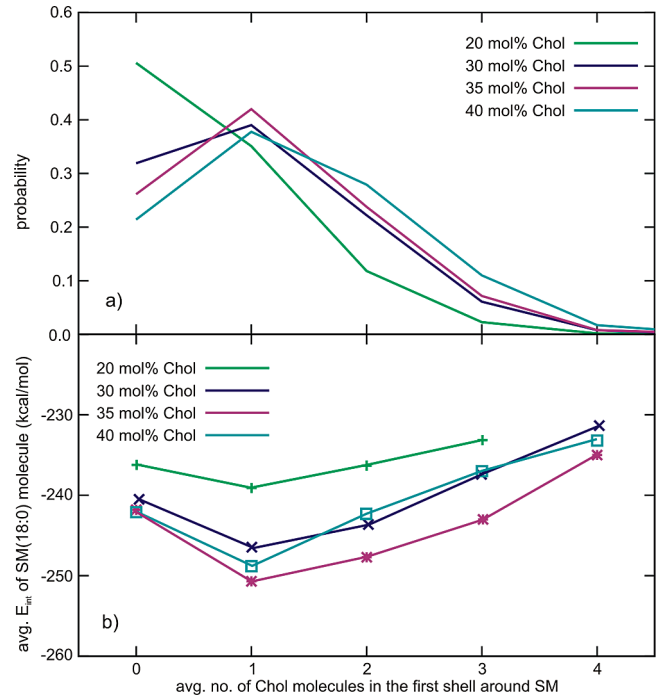

Figure 10. (a) Probability of sphingomyelin(18:0) having a given number of cholesterol neighbors in the first shell around the sphingomyelin molecule. (b) Average interaction energy in (kcal/mol) for sphingomyelin(18:0) with the rest of the model systems depending upon cholesterol concentration and number of cholesterol neighbors. The error bar is roughly 5%. Key: green, 20 mol % cholesterol; blue, 30 mol % cholesterol; violet, 35 mol % cholesterol; cyan, 40 mol % cholesterol.

In general, there are two principles that control the disposition of cholesterol and sphingomyelin in the bilayer. First, cholesterol molecules tend to leave regions of high local cholesterol concentration and move toward regions of low cholesterol concentration thus registering a gain in mixing entropy. Second, cholesterol molecules are attracted to regions which present a potential for hydrogen bonding and a consequent gain in enthalpy. At concentrations of cholesterol below 30 mol %, the entropy factor is controlling, but at concentrations above 30 mol %, the enthalpy factor is dominant.

Our results clearly show the tendency for formation of two different local environments in cholesterol/sphingomyelin bilayers above and below 30 mol % of cholesterol. This is consistent with the experimentally observed membrane activity of ostreolysin (Figure 1). This cytolytic protein interacts and permeabilizes the cholesterol/sphingomyelin membranes only when cholesterol concentration is above 30 mol %, suggesting that it could specifically bind to the lipid bilayer and interact with the liquid-ordered phase. This specific interaction is also in agreement with one of the proposed functions of lipid raft-like domains—specific sites for binding of various biological ligands. It should be noted that our results are indirect as the lipid bilayers were simulated without the protein ostreolysin. To gain further atomic insight and remedy this issue, further experimental work and simulations of lipid bilayers with the protein itself are needed, but only after the three-dimensional structure of the latter is determined. We have nevertheless observed a transition from a liquid-disordered to a liquid-ordered phase when increasing the molar concentration of cholesterol beyond 30%. In view of the agreement between the experimentally observed membrane activity of ostreolysin and the threshold concentration of cholesterol at which the liquid-ordered phase is formed, we simply speculate that ostreolysin might bind specifically to the liquid-ordered phase.

Conclusion

A series of all-atom molecular dynamics simulations of sphingomyelin(18:0) with different molar concentrations of cholesterol (0/100, 20/80, 30/70, 35/65, 40/60), started from randomly placed lipids in the bilayer planes, revealed significant structural features involved in formation of the liquid-ordered phase. The threshold cholesterol concentration at which the transition from the liquid-disordered phase to the liquid-ordered phase appears is approximately 30 mol %, which is in perfect agreement with the experimental results. The critical elements for different packing behaviors appear to be the interplay between interaction of sphingomyelin and cholesterol and interactions between different sphingomyelin molecules. Hydrogen bonding was found to be important in the concomitant formation of the liquid-ordered phase. Our results suggest that cholesterol/sphingomyelin mixing below 30 mol % is entropy-driven, while above 30 mol % it is enthalpy-driven.

Acknowledgment. The financial support through grants P1-0002 and P1-0207 of the Ministry of Higher Education, Science, and Technology of Slovenia and the Slovenian Research Agency is acknowledged.

References and Notes

(1) McConnell, H. M.; Vrljic, M. *Annu. Rev. Biophys. Biomol. Struct.* **2003**, *32*, 469–492.
(2) Lichtenberg, D.; Goñi, F. M.; Heerklotz, H. *Trends Biochem. Sci.* **2005**, *30*, 430–436.
(3) Rinia, H. A.; Snel, M. M.; van der Eerden, J. P.; de Kruijff, B. *FEBS Lett.* **2001**, *501*, 92–96.
(4) Pike, L. J. *Biochem. J.* **2004**, *378*, 281–292.
(5) Hancock, J. F. *Nat. Rev. Mol. Cell. Biol.* **2006**, *7*, 456–462.
(6) Sharma, P.; Varma, R.; Sarasij, R. C.; Ira; Gousset, K.; Krishnamoorthy, G.; Rao, M.; Mayor, S. *Cell* **2004**, *116*, 577–589.
(7) de Almeida, R. F. M.; Loura, L. M.; Fedorov, A.; Prieto, M. *J. Mol. Biol.* **2005**, *346*, 1109–1120.
(8) Subczynski, W. K.; Kusumi, A. *BBA - Biomembranes* **2003**, *1610*, 231–243.
(9) Kenworthy, A. K.; Petranova, N.; Edidin, M. *Mol. Biol. Cell* **2000**, *11*, 1645–1655.
(10) Simons, K.; Ikonen, E. *Nature* **1997**, *387*, 569–572.
(11) London, E. *Curr. Opin. Struct. Biol.* **2002**, *12*, 480–486.
(12) Edidin, M. *Annu. Rev. Biophys. Biomol. Struct.* **2003**, *32*, 257–283.
(13) Ishitsuka, R.; Yamaji-Hasegawa, A.; Makino, A.; Hirabayashi, Y.; Kobayashi, T. *Biophys. J.* **2004**, *86*, 296–307.
(14) Kiyokawa, E.; Baba, T.; Otsuka, N.; Makino, A.; Ohno, S.; Kobayashi, T. *J. Biol. Chem.* **2005**, *280*, 24072–24084.
(15) Ohno-Iwashita, Y.; Shimada, Y.; Waheed, A. A.; Hayashi, M.; Inomata, M.; Nakamura, M.; Maruya, M.; Iwashita, S. *Anaerobe* **2004**, *10*, 125–134.
(16) Berne, S.; Križaj, I.; Pohleven, F.; Turk, T.; Maček, P.; Sepčić, K. *Biochim. Biophys. Acta* **2002**, *1570*, 153–159.
(17) Vidic, I.; Berne, S.; Drobne, D.; Maček, P.; Frangež, R.; Turk, T.; Štrus, J.; Sepčić, K. *Mycol. Res.* **2005**, *109*, 377–382.
(18) Rebolj, K.; Ulrih, N. P.; Maček, P.; Sepčić, K. *BBA - Biomembranes* **2006**, *1758*, 1662–1670.
(19) Sepčić, K.; Berne, S.; Rebolj, K.; Batista, U.; Plemenitaš, A.; Šentjurc, M.; Maček, P. *FEBS Lett.* **2004**, *575*, 81–85.
(20) de Almeida, R. F. M.; Fedorov, A.; Prieto, M. *Biophys. J.* **2003**, *85*, 2406–2416.
(21) Chowdhury, H. H.; Rebolj, K.; Kreft, M.; Zorec, R.; Maček, P.; Sepčić, K. *Toxicon* **2008**, *51*, 1345–1356.
(22) Chiu, S. W.; Vasudevan, S.; Jakobsson, E.; Mashl, R. J.; Scott, H. L. *Biophys. J.* **2002**, *83*, 1842–1853.
(23) Mombelli, E.; Morris, R.; Taylor, W.; Fraternali, F. *Biophys. J.* **2003**, *84*, 1507–1517.
(24) Filippov, A.; Oradd, G.; Lindblom, G. *Biophys. J.* **2003**, *84*, 3079–3086.
(25) Chiu, S. W.; Vasudevan, S.; Jakobsson, E.; Mashland, R. J.; Scott, H. L. *Biophys. J.* **2003**, *85*, 3624–3635.
(26) de Meyer, F.; Smit, B. *Proc. Natl. Acad. Sci. U.S.A.* **2009**, *106*, 3654–3658.
(27) Janežič, D.; Praprotnik M.; Merzel, F. *J. Chem. Phys.* **2005**, *122*, art. no. 174101.
(28) Pastor, R. W.; Venable, R. M.; Karplus, M. *Proc. Natl. Acad. Sci. U.S.A.* **1991**, *88*, 892–896.
(29) Högberg, C.-J.; Nikitin, A. M.; Lyubartsev, A. P. *J. Comput. Chem.* **2008**, *29*, 2359–2369.
(30) Pastor, R. W.; Venable, R. M.; Feller, S. E. *Acc. Chem. Res.* **2002**, *35*, 438–446.
(31) Heller, H.; Schaefer, M.; Schulten, K. *J. Phys. Chem.* **1993**, *97*, 8343–8360.
(32) Klauda, J. B.; Roberts, M. F.; Redfield, A. G.; Brooks, B. R.; Pastor, R. W. *Biophys. J.* **2008**, *94*, 3074–3083.
(33) Pandit, S. A.; Vasudevan, S.; Chiu, S. W.; Mashl, R. J.; Jakobsson, E.; Scott, H. L. *Biophys. J.* **2004**, *87*, 1092–1100.
(34) Khelashvili, G. A.; Scott, H. L. *J. Chem. Phys.* **2004**, *120*, 9841–9847.
(35) Pandit, S. A.; Jakobsson, E.; Scott, H. L. *Biophys. J.* **2004**, *87*, 3312–3322.
(36) Aittoniemi, J.; Niemelä, P. S.; Hyvönen, M. T.; Karttunen, M.; Vattulainen, I. *Biophys. J.* **2007**, *92*, 1125–1137.
(37) Niemelä, P. S.; Ollila, S.; Hyvönen, M. T.; Karttunen, M.; Vattulainen, I. *PloS Comput. Biol.* **2007**, *3*, 304–312.
(38) Brooks, B. R.; Bruccoleri, R. E.; Olafson, B. D.; States, D. J.; Swaminathan, S.; Karplus, M. *J. Comput. Chem.* **1983**, *4*, 187–217.
(39) Woolf, T. B.; Roux, B. *Proc. Natl. Acad. Sci. U.S.A.* **1994**, *91*, 11631–11635.
(40) Jorgensen, W. L. *J. Am. Chem. Soc.* **1981**, *103*, 335–340.
(41) Hoover, W. G. *Phys. Rev. A* **1985**, *31*, 1695–1697.
(42) Essman, U.; Perera, L.; Berkowitz, M. L.; Darden, T.; Lee, H.; Pedersen, L. G. *J. Chem. Phys.* **1995**, *103*, 8577–8593.
(43) Brooks, B. R.; Brooks, C. L., III; Mackerrell, A. D., Jr.; Nilsson, L.; Petrella, R. J.; Roux, B.; Won, Y.; Archontis, G.; Bartels, C.; Boresch, S.; Calfisch, A.; Caves, L.; Cui, Q.; Dinner, A. R.; Feig, M.; Fischer, S.; Gao, J.; Hodošček, M.; Im, W.; Kuczera, K.; Lazaridis, T.; Ma, J.; Ovchinnikov, V.; Paci, E.; Pastor, W. R.; Post, C. B.; Pu, J. Z.; Schaefer, M.; Tidor, B.; Venable, R. M.; Woodcock, H. L.; Wu, X.; Yang, W.; York, D. M.; Karplus, M. *J. Comput. Chem.* **2009**, *10*, 1545–1614.
(44) Merzel, F.; Hodošček, M.; Janežič, D.; Sanson, A. *J. Comput. Chem.* **2006**, *27*, 446–452.

(45) Feller, S. E.; Gawrisch, G.; MacKerell, A. D., Jr. *J. Am. Chem. Soc.* **2001**, *124*, 318–326.
(46) Feller, S. E.; MacKerell, A. D., Jr. *J. Phys. Chem. B* **2000**, *104*, 7510–7515.
(47) Schlenkrich, M.; Brickmann, J.; MacKerell, A. D., Jr.; Karplus, M. *Membranes: A Molecular Perspective from Computation and Experiment*, 1st ed.; Merz, M. K., Roux B., Eds.; Birkhäuser: Boston, 1996; pp 31−81.
(48) Borštnik, U.; Hodošček, M.; Janežič, D. *J. Chem. Inf. Model.* **2004**, *44*, 359–364.
(49) Humphrey, W.; Dalke, A.; Schulten, K. *J. Mol. Graph.* **1996**, *14*, 33–38.
(50) Maulik, P. R.; Sripada, P. K.; Shipley, G. G. *Biochim. Biophys. Acta* **1991**, *62*, 211–219.
(51) Vermeer, L. S.; de Groot, B. L.; Reat, V.; Milon, A.; Czaplicki, J. *Eur. Biophys. J.* **2007**, *36*, 919–931.

JP907138H